Light Metals 2011 *Edited by: Stephen J. Lindsay*
TMS (The Minerals, Metals & Materials Society), 2011

TOWARDS A BETTER UNDERSTANDING OF THE CARBURATION PHENOMENON

Martin Lebeuf[1], Marc-André Coulombe[1], Bénédicte Allard[2], Gervais Soucy[1].

[1]Département de génie chimique (REGAL), Université de Sherbrooke, 2500 boul. université, Sherbrooke, Qc, J1K2R1, Canada.
[2]Carbone Savoie, 30 rue Louis Jouvet BP 16, 69631 Vénissieux Cedex, France

Keywords: Aluminum Electrolysis, Aluminum Carbide Formation, Cathode Wear, XPS, XPS Imaging

Abstract

Cathode wear in aluminum electrolysis cells is an undesired phenomenon which decreases potlife. Although it has been the subject of many studies, it is not yet satisfactorily understood. Furthermore, one major factor of this wear is the formation and dissolution of aluminum carbide, for which the mechanisms also still remain to be thoroughly explained. In view of this, laboratory scale electrolysis experiments were performed under different operating conditions, namely the duration and the presence or absence of an aluminum metallic layer on the cathode surface. The aluminum carbide formation was then studied using tomography, optical microscopy, Scanning Electron Microscopy-Energy Dispersive Spectroscopy (SEM-EDS) and X-ray Photoelectron Spectroscopy (XPS). In particular, the XPS analysis permits further investigation of the chemical species present in bath-penetrated veins of the carbon cathode.

Introduction

The formation and dissolution of aluminum carbide (Al_4C_3) and its subsequent oxidation at the anode are known to be important mechanisms in regards to the erosion of the cathode blocks, according to the following simplified general mechanism. Initially, Al_4C_3 forms at the cathode-metal interface, i.e. on the cathode surface and in pores near the surface, according to the general reaction (1) [1].

$$4\ Al_{(l)} + 3\ C_{(s)} = Al_4C_{3\ (s,\ diss)} \qquad (1)$$

The carbide can then dissolve in the liquid metal in which it is slightly soluble (probably less than 0.01 wt% at reduction cell temperatures [2]). The much higher solubility of the carbide in molten cryolite (2.1 wt% at CR=1.8 and 1020°C) [3] suggests that the possible presence of a bath film at the cathode-metal interface could enhance its dissolution [4]. In any case, the carbide eventually reaches the electrolytic bath, where it is believed that it dissolves according to reaction (2) [3].

$$Al_4C_{3\ (s)} + 5\ AlF_{3\ (diss)} + 9\ NaF_{(l)} = 3\ Na_3Al_3CF_{8\ (diss)} \qquad (2)$$

Once the carbide is dissolved in the electrolyte, it can reach the anodic region by convection and diffusion and then be oxidized. The net effect is thus a loss of carbon at the cathode surface.

Among the electrolysis cell parameters known to influence the carbon cathode erosion rate, increased current density is the most important [4,5,6]. Some other known factors are higher aluminum metal pad velocity, excess alumina and higher AlF_3 content [5]. Furthermore, graphitized materials, increasingly used due to their improved properties, especially electrical, exhibit higher erosion rates [7].

In previous work [8], laboratory scale electrolysis experiments were performed to examine bath-filled pores near the cathode surface with X-Ray Photoelectron Spectroscopy (XPS). Inside and/or on the periphery of those pores, the analysis of the high resolution C 1s spectrum revealed the presence of C-Al and C-O-Al bonds. Those findings encouraged the authors to further investigate those supposed C-Al and C-O-Al bonds.

Although Al_4C_3 formation in the carbon cathode pores can be identified with relatively good confidence by optical microscopy (due to its characteristic yellow color) and by X-ray mapping (concordant carbon and aluminum signals suggest the presence of aluminum carbide) [9,10], the use of XPS is justified by the new information it can provide, which could help better understand the Al_4C_3 formation/dissolution mechanisms. Indeed, as shown in the previous work, it can confirm with very good confidence the presence of different chemical bonds such as C-Al. It can also allow mapping of the chemical elements as well as the chemical species.

In an effort to identify new tools to study the Al_4C_3 formation, some results provided by tomography will also be presented.

Experimental

Laboratory bench scale electrolysis experiments were performed within a cylindrical graphitic cathode crucible with dimensions, general operating conditions and sample preparation outlined in previous articles [8,11]. In order to study carbide formation, three experiments were performed using the parameters presented in Table 1. In one experiment, a layer of aluminum was initially placed on the cathode surface, but the post-experiment examination revealed that the cathode surface was not completely covered by the metal.

Table 1: Experimental Conditions

Run #	Cathode current density (A/cm^2)	Electrolysis time (h)	Initial presence of Al	Inert gas
1	0.8	5	No	N_2
2	0.8	7.3	No	N_2
3	0.8	7.3	Yes	N_2

For optical microscopy, SEM-EDS and XPS analysis of the cathode subsurface, small vertical pieces of the cathode were cut in order to obtain a surface perpendicular to the bath-cathode interface (Figure 1).

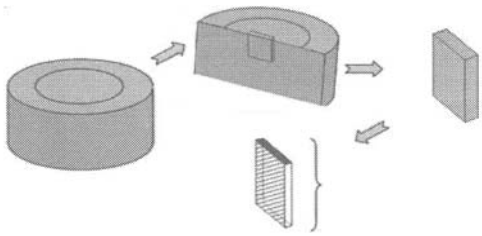

Figure 1: Perpendicular cross-section of the cathode: the grey area corresponds to the cathode surface and the striped area is the surface analyzed.

Tomography scans were performed with a Skyscan 1172 operating at 70 kV, 142 µA and using an Al-Cu filter. The camera was set at a resolution of 1000 x 500 pixels and an exposure time of 632 ms.

XPS analysis of the cathode material was performed using an AXIS ULTRADLD spectrometer (Kratos Analytical Ltd., Manchester, GB) equipped with a monochromatic Al Kα source operated at 225 W. The elemental composition of the analyzed surface areas was obtained from survey spectra collected at a pass energy of 160 eV. High-resolution C 1s and O 1s spectra were collected at 20 eV, but for the parallel imaging experiment, the equipment was set at 40 eV for intensity purposes. The pressure in the analytical chamber was lower than 10^{-6} Pa and the apparatus was calibrated against the following lines: Au 4f, Ag 3d and Cu 2p. Since the sample was charging, an electron flood gun was used during the XPS experiments. Atomic concentrations of each component were calculated using CasaXPS (Casa Software Ltd.) by determining the relevant integral peak areas; a Shirley background was used. To compare the high-resolution C 1s, O 1s and Al 2p peak positions, the spectra were calibrated in reference to the fitted graphitic C-C component at 284.5 eV. The detailed spectra were fitted with several peaks using a Lorentzian asymmetric lineshape with tail damping for the graphitic C-C and a mixed Gaussian-Lorentzian function for other components.

Results and Discussion

Tomography

Tomography scans were generated to monitor the penetration depth and penetration depth profile in a specified location within the cathode blocks (Figure 2). It is known that cryolite might react with the cathode block carbon and intercalated sodium according to reaction (3).

$$4\ Na_3AlF_{6\,(l)} + 12Na_{\,(inC)} + 3C_{\,(s)} = Al_4C_{3\,(s)} + 24NaF_{\,(l)} \qquad (3)$$

In view of this reaction, it was relevant to measure the bath penetration front. Visual observations of bath penetration are, though, somehow imprecise. For instance, because of preferential paths caused by cracks and porosities, bath infiltrations much deeper than the true bath penetration front can be seen. A more accurate method was desired, and the tomography scans provided a rapid and reliable way to confirm the true depth of the bath penetration front. Furthermore, it allowed a 3-D analysis, instead of the visual surface observations. Each tomography scan required only five minutes to acquire and process.

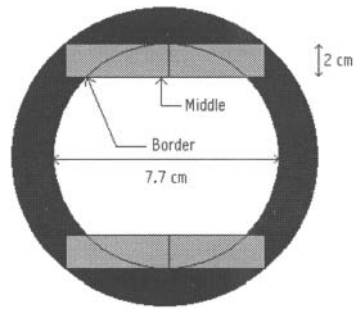

Figure 2: View (from above) of the cathode crucible, with cathode surface in white, cathode walls in black and position of the sawn-off pieces analyzed by tomography in grey.

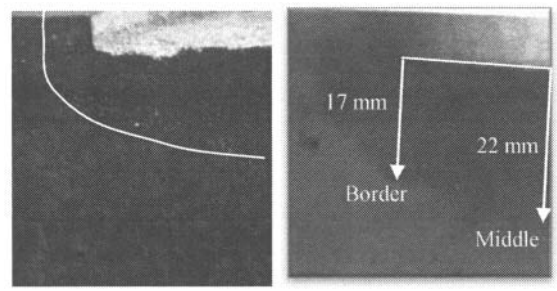

Figure 3: Tomography scan (right) of a crucible piece from test #3, showing the bath penetration profile. The carbon cathode block size is 60 mm long by 35 mm large by 20 mm deep. The cathode surface is visible in the upper right part of the image.

The bath penetration profile can be seen in the right part of Figure 3, the darker area being bath-impregnated. The density and composition of bath versus graphitic carbon causes this zone to be less transparent to the x-rays. It is then possible to measure the distance between the cathode surface and the bath front. Comparisons between the tests were made by measuring the bath front depth at two different positions for each sample: beneath the cryolite/cathode wall border (left arrow, Figure 3) and the middle of the cathode surface (right arrow, Figure 3). Penetration depth values typically ranged from 5 to 25 mm. The measurements from the three tests resulted in average penetration rates of 1.7 mm/h and 2.6 mm/h for the wall and middle regions, respectively.

SEM-EDS

A bath-impregnated vein right beneath the cathode surface, from a sample taken from test #2 (as described in Figure 1), was analyzed by optical microscopy (Figure 4), SEM-EDS (Figures 4-5) and XPS (Figures 7-11). The optical microscope image shows the yellow carbide layer on the cathode surface and on the vein edges.

The X-ray elemental mapping acquired (Figure 5) reveals a strong Al presence in the carbide layer. The C, F and Na elements are present as expected, with some expected Na in the graphitic matrix. As for Ca, its non-homogeneous distribution in the vein can probably be attributed to the crystallization of the different Ca-species. The strongest presence of O appears to be linked with the Al element, i.e. in the carbide layer. Such a result was reported previously in the literature. Xue and Øye [12] suggested that the carbides could have reacted with alumina to generate oxycarbides,

according to reactions (4) and (5). Patel et al. [10] suggested that it could be alumina formed by the hydrolysis of aluminum carbide, according to reactions (6) and (7). Zoukel et al. [11] suggested that handling of the sample in air could have allowed reaction (6) to take place, or that, simply, alumina could have deposited on the surface during cooling.

$$Al_4C_{3\,(s)} + Al_2O_{3\,(s)} = 3Al_2OC_{(s)} \quad (4)$$

$$Al_4C_{3\,(s)} + 4Al_2O_{3\,(s)} = 3Al_4O_4C_{(s)} \quad (5)$$

$$Al_4C_3 + 6O_2 = 2Al_2O_3 + 3CO_2 \quad (6)$$

$$Al_4C_3 + 6H_2O = 2Al_2O_3 + 3CH_4 \quad (7)$$

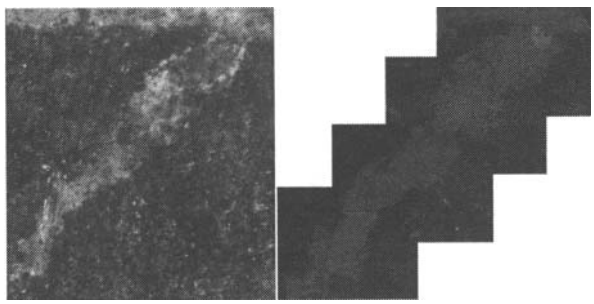

Figure 4: Optical microscopy (left) and SEM back-scattered electron (right) images of a bath-impregnated vein beneath the cathode surface from test #4.

About oxycarbides, Grjotheim et al. [13], in 1978, identified Al_2OC in the reaction product of alumina, cryolite and aluminum placed in a graphite crucible and kept for 12 hours at 1050°C and for another 24 hours at 975°C (no electrolysis was performed). Since then, in the literature related to the Hall-Heroult process, there has not been significant reported indications of the presence of oxycarbides in laboratory or industrial alumina reduction cells (at cooled temperatures, where chemical analysis are possible). Chryssoulakis and Righas [14] did, in an electrochemical study performed at 1300K in acidic cryolitic baths with alumina additions, suggest that the observed reoxidation peaks could be due to the oxycarbides compounds Al_2OC and Al_4O_4C. These two oxycarbide compounds were first described and studied by Foster et al. in 1956 [15]. It seems relevant to indicate that since then, even though it has been described and studied in different works [16,17,18], the very existence of thermodynamically stable Al_2OC has been put in serious doubt [19]. In any case, either stable or metastable, this Al_2OC compound should not, as pointed out by Lihrmann [20], be observed in significant amounts in an aluminum reduction cell, since it was shown to exist only at temperatures between 1715°C and 2000°C. Ødegard [3], in his study of the solubility of Al_4C_3 in cryolitic melts at reduction cell temperatures, also did not see any indication of the occurrence of this compound.

Therefore, the presence of oxygen in the carbide layer seen in Figure 6 can probably be attributed to Al_2O_3 and/or Al_4O_4C. Since XPS results obtained in a previous work [8] suggested the presence of oxycarbide species in bath-impregnated pores of the cathode, reaction (5) should be of some importance. No thermodynamic analysis has been conducted for the moment to further investigate the matter.

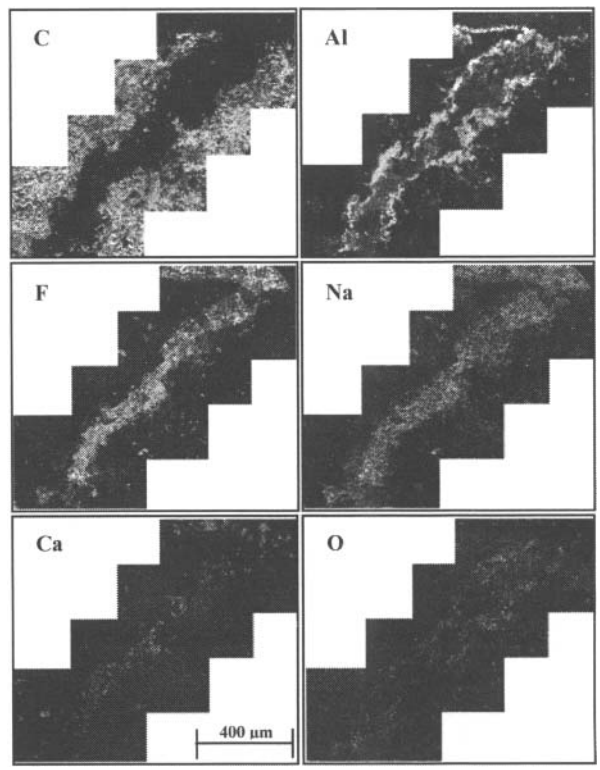

Figure 5: Bath-infiltrated vein from test #2 : EDS mapping of a) C, b) Al, c) F, d) Na, e) Ca and f) O.

XPS C 1s high resolution spectrum interpretation

The analysis and deconvolution of a high-resolution XPS spectra can be quite complex and the present study required some further investigation. In the literature, many authors have identified C-Al and C-O-Al bonds in the high resolution C 1s spectrum [21,22,23,24,25], but the majority of these studies were performed on homogeneous, pristine surfaces, mostly made by the deposition of a thin film of aluminum on a material by evaporation, sputtering, or chemical reaction. Furthermore, those thin films were often etched to various degrees for surface bondings analysis and so the very last layers of deposited metal were analysed. This fact is mentioned since one can expect the C-Al and C-O-Al species or complexes formed by those methods to be different from the crystalline Al_4C_3 expected in the carbon cathode. Nevertheless, in both cases the BE (binding energy) values for specific chemical bonds should be similar, and those values are discussed below.

In general, in the above-mentioned literature, the XPS charge effect is compensated by calibrating the energy scale in reference to the C-C bond of the C 1s at a BE value between 284.2 eV and 285.0 eV. This C-C bond can originate from different types of molecular arrangements (aliphatic versus aromatic, for example), which might explain this relatively large range of BE values. In the present study, as mentioned earlier, a value of 284.5 eV for the graphitic C-C bond of the C 1s was used. This is not true for the spectra presented in Figure 6 though, where no charge effect corrections were performed. Graphite was not always present in sufficient amounts to allow a reliable correction.

In the C 1s high resolution spectrum, the various XPS studies mentioned in the previous paragraphs attributed a C-O-Al complex at BE values between -1.2 eV and -1.6 eV relative to the C-C bond. It is noteworthy that a true linear chemical bond C-O-Al, where the carbon atom is directly linked to the O atom, should rather appear at a higher binding energy than the C-C bond, since the O is far more electronegative than either C or Al [25]. In other words, depending on its exact chemical structure, a C-O-Al species could be found on both energy sides of the C-C bond.

As for the C-Al bond, the above-mentioned literature suggests it should appear at BE values from -2.1 eV to -2.6 eV relative to the C-C bond.

In order to verify those C-Al BE values in the presence of a graphitic C-C bond peak (versus other types of C-C bonds), powders of Al_4C_3 and graphite were mixed at different concentrations and analysed by XPS (the Al_4C_3 powder, >99% pure, was obtained from Alfa Aesar and the graphitic powder was obtained by crushing pieces of the graphitic cathode materials). The results are shown in Figure 6. The dotted lines are added to help compare the major peaks from the different spectra.

It is worth mentioning that there is in principle no true chemical C-C bonds in pure Al_4C_3, since in its complex crystal structure the closest distance between two carbon atoms is 316 pm [26].

In spectrum (a) of Figure 6, the characteristic graphitic C 1s appears as expected. In spectrum (b), a mixture of 50 wt% graphite and 50 wt% Al_4C_3 reveals that the graphitic C 1s peak is still dominant, but has shifted about -0.5 eV, probably due to the apparition of the C-Al peak (still mostly hidden by the graphitic C-C peak). In spectrum (c), the top of the two peaks are separated and the graphitic peak is back to its 284.5 eV BE value. In spectrum (d), with only slightly higher Al_4C_3 concentration, the graphitic peak has almost disappeared beneath the C-Al peak. From spectra (c-d), the calculated BE difference between the C-Al and the graphitic C-C is -2.2 ± 0.1 eV, in good agreement with the above-mentioned values. The (e) spectrum shows almost no sign of graphite although it represents 20 wt% of the sample, and the last spectrum (f) shows the 100 wt% Al_4C_3.

The two small peaks at low BE values that can been seen in (e) and (f) and partly in (b), (c) and (d), at about -1.9 ± 0.1 eV and -3.2 ± 0.1 eV relative to the C-Al bond, remained unidentified. Itatani et al. [27] studied Al_4C_3 powders produced by different methods, and the XPS spectra they obtained were quite similar to the one obtained in the present work (f). They suggested the small peaks at low BE values to be caused by alkylaluminum radicals still present in the powder after the reactions steps used to produce Al_4C_3. The current study is concerned with those peaks since XPS spot-checks performed on bath-impregnated pores of a cathode in a previous work showed peaks appearing at lower BE values than expected for C-Al and C-O-Al.

The presented spectra and approximate BE values still consist in a preliminary evaluation. A complete deconvolution of the high resolution C1s peak, as well as the Al 2p and O 1s peaks (which are more complex, since their respective peaks are less separated), will be necessary to properly characterise the species and draw conclusions. Moreover, the XPS analysis of a bath-impregnated cathode is further complicated by its non-homogeneous nature, which can possibly induce localised charge effects (bath zones versus graphite zones). It can also be difficult to know the exact, precise location of an XPS scan when very small areas are scanned.

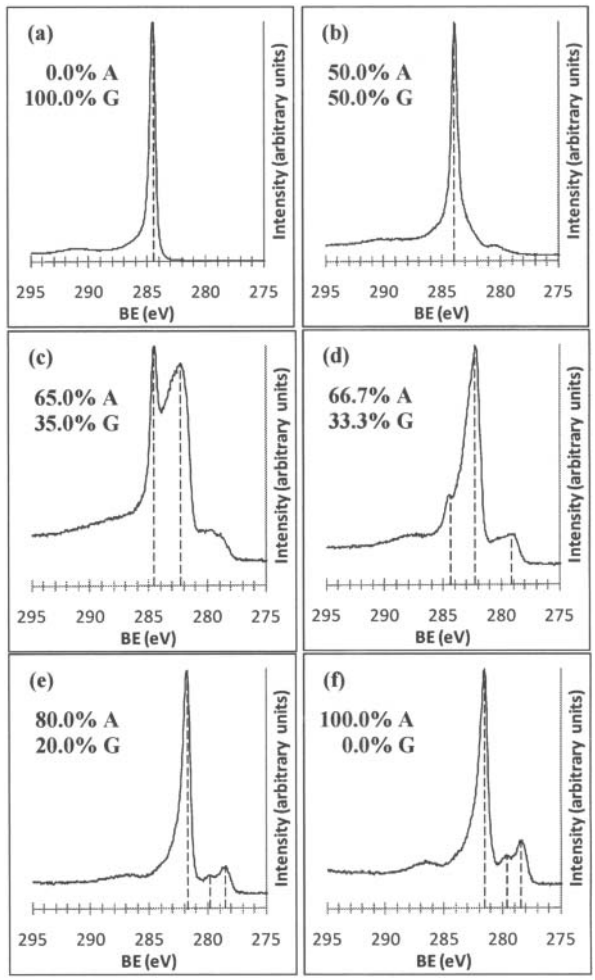

Figure 6: C 1s High resolution XPS spectra of powders with different Al_4C_3 (A) and graphite (G) mass concentrations. Scans were performed at a pass energy of 20 eV, a dwell time of 250 ms and 5 sweeps. No charge effect corrections were made.

To further investigate the carbide and the so called oxycarbide chemical species in the bath-impregnated cathode, XPS imaging was used to isolate those peaks from the C 1s spectrum. The technique consisted of collecting an image of 128 x 128 pixels and transforming this image to the according number of spectra. Those spectra were divided into regions that corresponded to C-F (286.0 – 288.0 eV), graphitic C-C (284.0 – 285.5 eV), C-O-Al (282.0 – 284.0 eV) and C-Al (281.0 - 282.5 eV) bonds. These regions were converted to an image. Because of the presence of a cryolite vein going through the carbon matrix, the regions gave different images according to their intensity. Dividing the intensity scale in relevant ranges called false color (Figures 7-8), the pixel spectra were sorted to generate a representative spectrum of each bond.

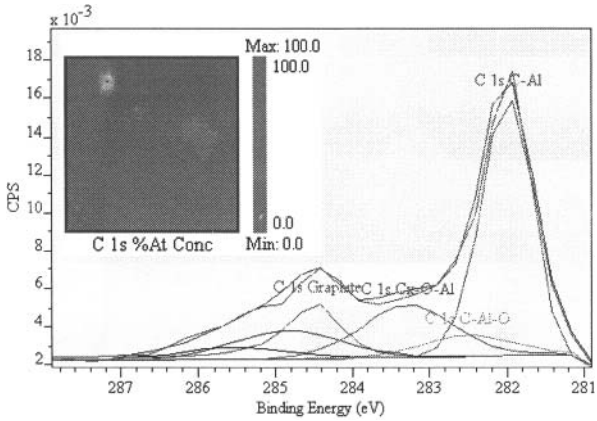

Figure 7: False color spectrum showing the shape and position of the C-Al bond. The averaged spectra are from the gold region.

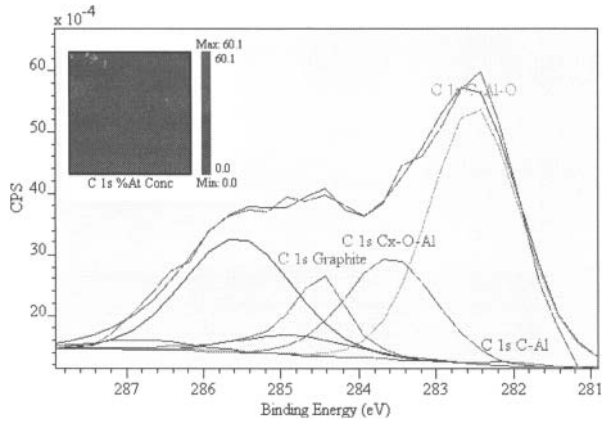

Figure 8: False color spectrum showing the shape and position of the C-O-Al bond. The averaged spectra are from the gold region.

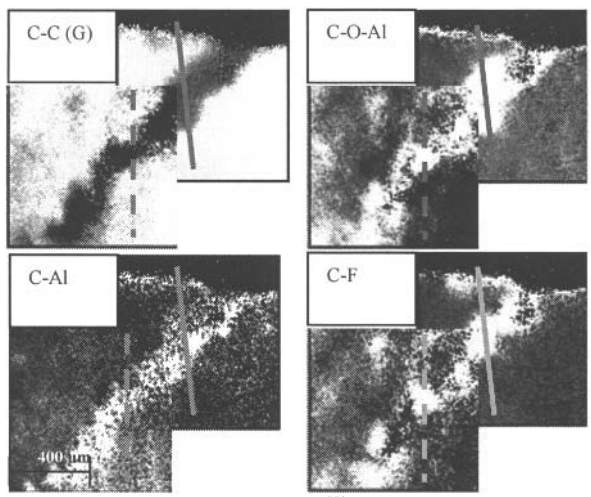

Figure 9: XPS imaging of the vein from test #4.

By averaging all spectra from the gold region (called false color model), Figure 7 clearly isolates the major C-Al peak and shows evidence of Al_4C_3 (see Figure 6). Figures 7-8 reveal the existence of two different C-O-Al bonds represented by one line scan since they cannot be isolated from each other in any part of the image. Figure 9 shows the results associated with the region model development. The graphitic C-C image corroborates Figures 4-5, while C-O-Al, C-Al and C-F bond imaging is new information. The new bond is assumed to be C-F because of its BE of 287.7 eV, but this still needs to be confirmed with element imaging. The presence of that bond was established using the same strategy of averaging spectra of another false color region as demonstrated in Figures 7-8 for C-Al and C-O-Al, respectively.

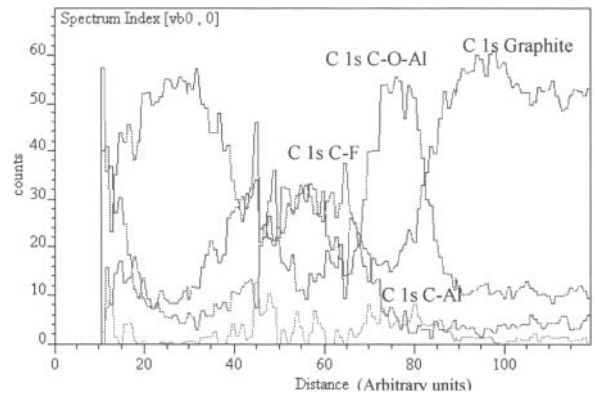

Figure 10: First set of linescans (see Figure 9, full lines), showing relative concentrations of the different C 1s bonds.

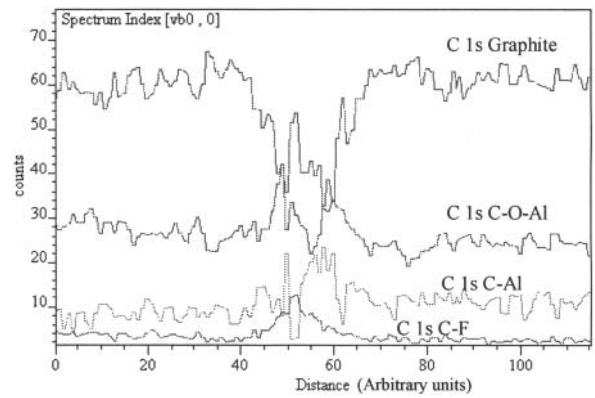

Figure 11: Second set of linescans (see Figure 9, dashed lines), showing relative concentrations of the different C 1s bonds.

It is difficult, from XPS imaging (Figure 9), to interpret the different bonds distribution since they are solely based on an intensity scale. Linescans (Figures 10-11), however, enable comparison with counts that are proportional to concentration within the C 1s spectrum. From those results, it is made clear that in the vein, the supposed C-O-Al, C-Al and C-F bonds exist while there is a much lower level of graphitic C-C bond than in the cathode matrix. The linescans also reveal differences in the distribution of the various chemical bonds within the vein (it seems relevant to indicate that for such XPS imaging, the resolution is about 3 µm, or 0.5 arbitrary units on the line scan abscissa). However, a band larger than 281.0 to 288.0 eV should have been used to fit a proper background and thus obtain less noisy results. More obvious gradients were observed before [8], but the vein observed in the present work is considerably thinner.

Conclusions

Three experiments were conducted in order to investigate the formation of aluminum carbide during the reduction of alumina in a cryolite-containing graphite crucible laboratory electrolysis cell.

Tomography analysis of carbon cathode samples from lab-scale experiments allowed quick and reliable determination of the bath penetration front depth.

Investigation of the XPS high resolution C 1s spectrum helped confirm the BE value of C-Al and revealed the presence of unknown species in a commercial grade Al_4C_3 powder. XPS imaging allowed to observe various chemical bonds and difference in their distribution in a bath-impregnated cryolite vein.

Future Work

The deconvolution of the high resolution C 1s, Al 2p and O 1s spectra for pure Al_4C_3 and spot-checks of bath-impregnated cathode samples still needs to be fully performed. This will allow the formal identification and quantification of the different compounds, which may include an oxycarbide. The refinement of the XPS imaging technique will reveal more precisely the distribution of the different chemical bonds. Combined with the analysis of bath-impregnated cathode pores from different electrolysis conditions, this information will be used to propose reaction mechanisms for the Al_4C_3 formation.

Acknowledgements

Financial support from the Fonds Québécois de la Recherche en Nature et Technologie (FQRNT) is gratefully acknowledged.

We are grateful to Sonia Blais and Irène Kelsey-Lévesque from the Centre of Characterization Materials (CCM) of the Université de Sherbrooke for the tomography, SEM-EDS and XPS analysis.

A special appreciation is given to Neal Fairley for his support with mapping curve synthesis using CasaXPS software.

Pure aluminum was provided by Neuman Aluminium Canada.

References

1. Morten Sørlie and Harald A. Øye, *Cathodes in Aluminium Electrolysis*, Düsseldorf, Aluminium-Verlag, 2nd ed.(1994), 408 p.
2. R. C. Dorward, "Aluminium Carbide Contamination of Molten Aluminium," *Aluminium*, 49 (1973), 686-689.
3. R. Ødegard, "On the Solubility of Aluminum Carbide in Cryolitic Melts," *Metallurgical and Materials Transactions B, 19 (1988)*, 441-447.
4. K. Vasshaug et al. "Formation and Dissolution of Aluminium Carbide in Cathode Blocks," *Light Metals 2009*, TMS,1111-1116.
5. S. Wilkening and P. Reny. "Erosion Rate Testing of Graphite Cathode Materials," *Light Metals 2004*, TMS, 597-602.
6. H. A. Øye et al. "Cathode Bottom Wear During Aluminum Electrolysis," *The Electrochemical Society*, 2002, 847-856.
7. D. Lombard et al. "Aluminium Pechyney Experience With Graphitized Cathode Blocks," Light Metals 1998, TMS, 653-658.
8. M.-A. Coulombe et al. "Carburation Phenomenons at the Cathode Block/Metal Interface", Light Metals 1010, 811-816.
9. O. Herstad et al. "Precipitation of Alumina and Aluminium Carbide During Electrolysis of Cryolite-Alumina Melts," *Light Metals 1983*, TMS, 347-356.
10. P. Patel et al. "Influence of Cathode Structure on Behavior During Electrolysis Part II: Porosity and Wear Mechanisms in Graphitized Cathode Material," *Light Metals 2005*, 757-762.
11. A. Zoukel et al. "Study of Aluminum Carbide Formation in Hall-Heroult Electrolytic Cells," *Light Metals 2009*, TMS, 1123-1128.
12. J. Xue amd and H. A. Øye. "Al_4C_3 Formation at the Interface of Al - Graphite and Al - Carbon/TiB2 Composite," *Light Metals 1994*, TMS, 211-217.
13. K. Grjotheim et al. "Aluminium Carbide and Oxy-carbide Formation in Alumina-Containing Cryolite Melts," *Light Metals 1978*, 107-117.
14. Y. Chryssoulakis and G. Righas. "Étude électrochimique des réactions d'oxydoréduction des carbures ou oxycarbures d'aluminium dans les bains cryolithiques acides additionnés d'alumine à 1300 K," *Bulletin de la Société chimique de France*, 1990, no. 5, 635-640.
15. L.M. Foster et al. "Reactions Between Aluminum Oxide and Carbon - The Al_2O_3-Al_4C_3 Phase ", *Journal of the American Ceramic Society*, 1956, vol. 39, no. 1, 1-11.
16. M. Heyrman and C. Chatillon. "Thermodynamics of the Al-C-O System", *Journal of the Electrochemical Society*, 2006, vol. 153, no. 7, E119-E130.
17. R. Yu et al. "Elastic constants and tensile properties of Al_2OC by density functional calculations," *Physical Review B*, 2007, vol. 75, no. 10, 104114-1-104114-5.
18. J.-M. Lihrmann. "Thermodynamics of the Al_2O_3-Al_4C_3 system I. Thermochemical functions of Al oxide, carbide and oxycarbides between 298 and 2100 K", *Journal of the European Ceramic Society*, 2008, vol. 28, 633-642.
19. K. Motzfeldt. "Comment on Thermodynamics of the Al-C-O System [J. Electrochem. Soc., 153, E119 (2006)]", *Journal of the Electrochemical Society*, 2007, vol. 154, no. 3, S1-S2.
20. J.-M. Lihrmann. "High-Temperature Behavior of the Aluminum Oxycarbide Al_2OC in th eSystem Al_2O_3-Al_4C_3 and with Additions of Aluminum Nitride", *Journal of the American Ceramic Society*, 1989, vol. 72, no. 9, 1704-1709.
21. B. M. DeKoven and J. M. White. "XPS Studies of Metal-Polymer Interfaces – Thin Films of Al on Polyacrylic Acid and Polyethylene," *Applied Surface Science*, 1986, vol. 27, 199-213.
22. S. Akhter et al. "XPS Study of Polymer/Organometallic Interaction : Trimethyl Aluminum on Polyvinyl Alcohol Polymer," *Applied Surface Science*, 1989, vol. 37, 201-216.
23. B. Maruyama et al. "Catalytic Carbide Formation at Aluminium-Carbon Interfaces," *Journal of Materials Science Letters*, 1990, vol. 9, 864-866.
24. C. Hinnen et al. "An in situ XPS Study of Sputter-Deposited Aluminium Thin Films on Graphite," *Applied Surface Science*, 1994, vol. 78, 219-231.
25. L. Sandrin and E. Sacher, "X-Ray Photoelectron Spectroscopy Studies of the Evaporated Aluminum/Corona-Treated Polyethylene Terephthalate Interface," *Applied Surface Science*, 1998, vol. 135, 339-349.
26. Norman Greenwood and A. Earnshaw. Chemistry of the Elements, Second Edition, Butterworth Heinemann, 1997, 297.
27. K. Itatani et al. "Some Properties of Aluminum Carbide Powder Prepared by the Pyrolysis of Alkylaluminum," *Journal of the American Ceramic Society*, 1995, vol. 78, no. 3, 801-804.